Bioconjugate Chemistry

Article

pubs.acs.org/bc

PET Imaging of Extracellular pH in Tumors with ^{64}Cu- and ^{18}F-Labeled pHLIP Peptides: A Structure−Activity Optimization Study

Dustin Wayne Demoin,[†] Linden C. Wyatt,[‖] Kimberly J. Edwards,[†] Dalya Abdel-Atti,[†] Mirkka Sarparanta,[†] Jacob Pourat,[†] Valerie A. Longo,[§] Sean D. Carlin,[†,‡] Donald M. Engelman,[⊥] Oleg A. Andreev,[‖,⊥] Yana K. Reshetnyak,[‖,⊥] Nerissa Viola-Villegas,[#] and Jason S. Lewis*[,†,‡,¶]

[†]Department of Radiology, [‡]Program in Molecular Pharmacology, and [§]Small-Animal Imaging Core Facility, Memorial Sloan Kettering Cancer Center, 1275 York Avenue, New York, New York 10065, United States

[‖]Physics Department, University of Rhode Island, 2 Lippitt Road, Kingston, Rhode Island 02881, United States

[⊥]pHLIP, Inc, 2 Lippitt Road, Kingston, Rhode Island 02881, United States

[#]Department of Oncology, Karmanos Cancer Institute, Detroit, Michigan 48201, United States

[¶]Weill Cornell Medical College, 1300 York Avenue, New York, New York 10065, United States

Supporting Information

ABSTRACT: pH (low) insertion peptides (pHLIP peptides) target acidic extracellular environments in vivo due to pH-dependent cellular membrane insertion. Two variants (Var3 and Var7) and wild-type (WT) pHLIP peptides have shown promise for in vivo imaging of breast cancer. Two positron emitting radionuclides (^{64}Cu and ^{18}F) were used to label the NOTA- and NO2A-derivatized Var3, Var7, and WT peptides for in vivo biodistribution studies in 4T1 orthotopic tumor-bearing BALB/c mice. All of the constructs were radiolabeled with ^{64}Cu or [^{18}F]-AlF in good yield. The in vivo biodistribution of the 12 constructs in 4T1 orthotopic allografted female BALB/c mice indicated that NO2A-cysVar3, radiolabeled with either ^{18}F (4T1 uptake; 8.9 ± 1.7%ID/g at 4 h p.i.) or ^{64}Cu (4T1 uptake; 8.2 ± 0.9%ID/g at 4 h p.i. and 19.2 ± 1.8% ID/g at 24 h p.i.), shows the most promise for clinical translation. Additional studies to investigate other tumor models (melanoma, prostate, and brain tumor models) indicated the universality of tumor targeting of these tracers. From this study, future clinical translation will focus on ^{18}F- or ^{64}Cu-labeled NO2A-cysVar3.

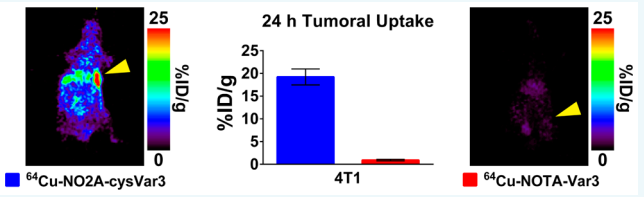

INTRODUCTION

Cancer cells, in general, prefer the glycolytic pathway of energy production as a consequence of their deregulated proliferative machinery and requirement for survival, resulting in excess acidity. To maintain homeostasis, cancer cells release lactic acid, formed during glycolytic processes, to the extracellular environment.[1−3] The release of acid lowers the extracellular pH immediately surrounding these cells relative to the pH of normal tissues. Due to the differential in pH gradients, a probe marking these acidic regions in rapidly proliferating tissues can potentially distinguish cancerous from normal tissue.

The family of pH (low) insertion peptides (pHLIP peptides) represents a novel class of delivery agents which can target acidic malignant tissue.[4,5] The molecular mechanism of targeting is based on the pH-dependent formation of a transmembrane α-helix, which is accompanied by the insertion of pHLIP peptides into the cellular membrane in environments with low extracellular pH (Figure 1).[6] Among investigated pHLIP variants, three were under consideration for clinical translation: wild-type (WT), variant 3 (Var3), and variant 7 (Var7).[7]

To date, pHLIP peptides have been conjugated to organic dyes or positron-emitting radioisotopes for in vitro and in vivo studies.[7−11] Viola-Villegas et al. showed that DOTA-pHLIP variants were able to target PC3-WT cancer cells in a pH-dependent manner using ^{68}Ga-DO3A-cysWT and ^{68}Ga-DO3A-cysVar7.[12] Additionally, ^{64}Cu-NOTA-Var7 showed in vivo localization that was inversely related to measured extracellular pH (pH_e), but with limited overall tumor uptake (1.36 ± 0.43% ID/g).[12]

The selection of NOTA as the chelator in the present studies opened opportunities to explore radiolabeling strategies with a variety of positron-emitting radiometals, as well as with ^{18}F, for positron emission tomography (PET) imaging.[13−16] As the previous studies with pHLIP-PET radiopharmaceuticals in preclinical models established the proof-of-principle that the pHLIP platform can indeed selectively target and image tumor acidosis, our goals have now advanced to performing first-in-human trials. It was first imperative, however, to optimize the

Received: June 13, 2016
Revised: July 5, 2016
Published: July 9, 2016

DOI: 10.1021/acs.bioconjchem.6b00306
Bioconjugate Chem. 2016, 27, 2014−2023

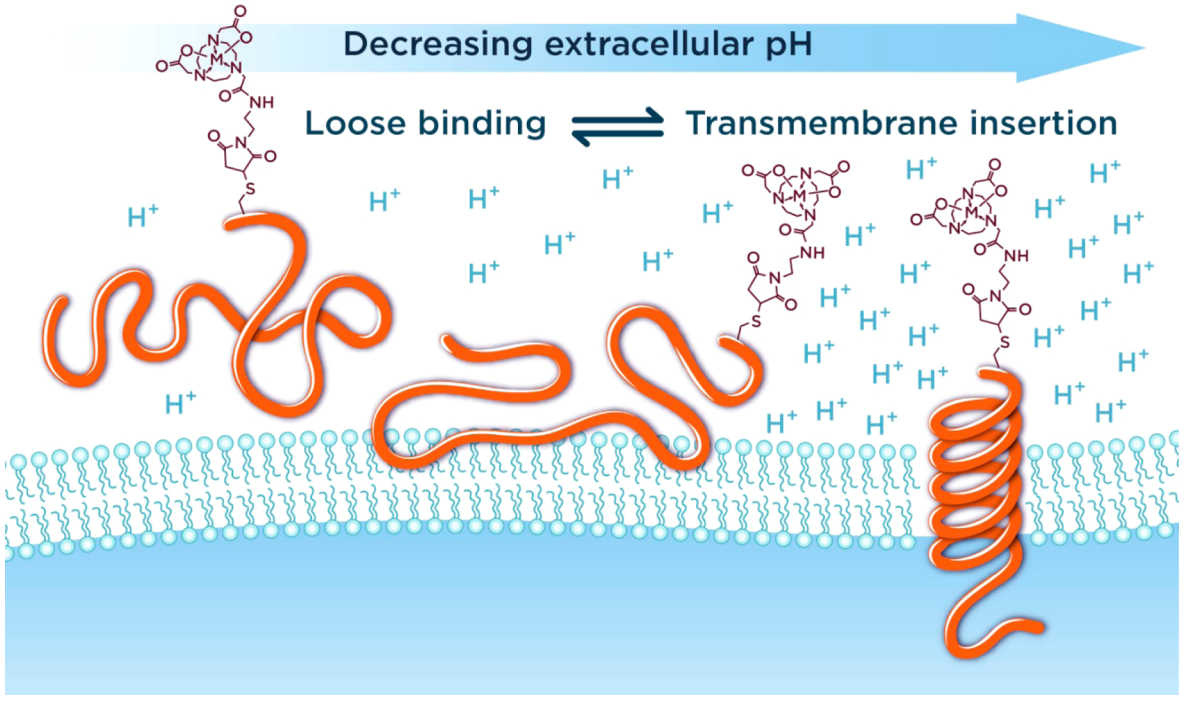

Figure 1. Three folding states of pHLIP peptides in decreasing extracellular pH: unfolded and unbound peptide in solution (State I), unfolded peptide loosely interacting with the membrane lipid bilayer at physiological pH (State II), and folded peptide in α-helical conformation inserted across the membrane at low extracellular pH (State III).

tracer (increasing accumulation in the tumor with a concomitant clearance from nontarget tissues) by careful selection of the optimal radioisotope and pHLIP peptide variant combination prior to commencing clinical studies.

In this current study, we investigated and compared the pharmacokinetic properties of six pHLIP constructs (NOTA-WT, NOTA-Var3, NOTA-Var7, NO2A-cysWT, NO2A-cysVar3, and NO2A-cysVar7) labeled with two different PET isotopes (^{64}Cu and ^{18}F) using an orthotopic breast cancer model (murine 4T1 mammary adenocarcinoma, a model of human stage IV breast cancer) through ex vivo biodistribution and in vivo imaging studies. In addition, the biophysical measurements of the nonradioactive, metalated peptides were conducted to help explain the variations observed in the animal studies. From these studies, two lead radiopharmaceuticals (^{18}F-AlF-NO2A-cysVar3 and ^{64}Cu-NO2A-cysVar3) were selected and further assessed in melanoma, prostate, and brain tumor models.

RESULTS

Preparing the Radiotracers. The NOTA (1,4,7-triazacyclononane-*N*′,*N*″,*N*‴-triacetic acid) chelator was conjugated to the pHLIP variants in two ways (Figure 2). The NOTA-pHLIP compounds contain NOTA with three carboxylic acid groups conjugated to the N-terminus of the peptide (Figure 2A). The NO2A-cyspHLIP compounds contain NOTA with two carboxylic acid groups, where the third group was used to conjugate the chelator to the peptide through the cysteine side chain (Figure 2B). The Cu^{2+} and AlF^{2+} NOTA complexes have an overall charge of −1 with a neutral charge at the N-terminus of the pHLIP peptides. All complexes with the NO2A-chelates have an overall neutral charge with the positive charge preserved at the N-terminus of the pHLIP peptides. The three peptide sequences are tabulated in Figure 2C.

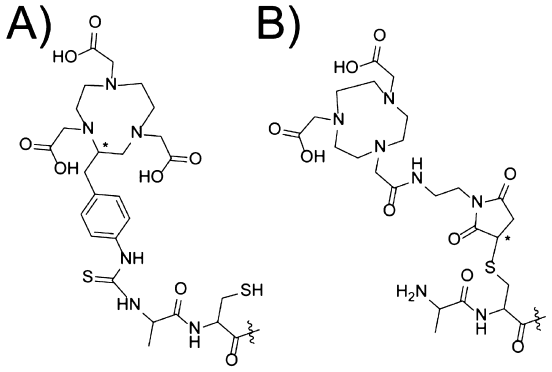

Peptide	Sequence
WT	ACEQNPIYWARYADWLFTTPLLLLDLALLVDADEGT
Var3	ACDDQNPWRAYLDLLFPTDTLLLDLLW
Var7	ACEEQNPWARYLEWLFPTETLLLEL

Figure 2. Two chelators [(A) NOTA-pHLIP and (B) NO2A-cyspHLIP] and (C) the peptide sequences used in this study. The chiral centers within the chelator and linker are marked with asterisks.

The ^{64}Cu radiolabeling of each of the conjugates was achieved with >60% (isolated) yield with >93% purity (Supporting Information); the ^{18}F-AlF radiolabeling of each of the conjugates was 4−50% (isolated and decay corrected to start of synthesis) yield with >95% purity (Supporting Information). Table S1 lists the specific activity of each radiolabeled pHLIP peptide.

In Vivo Studies in 4T1 Tumor Models. Direct evaluation of all 12 tracers in vivo was carried out in 4T1 orthotopic (surgically implanted) allografted female BALB/c mice in order to determine which compounds would be best translated into clinical studies. Figure 3 shows the in vivo PET imaging slices at

DOI: 10.1021/acs.bioconjchem.6b00306
Bioconjugate Chem. 2016, 27, 2014−2023

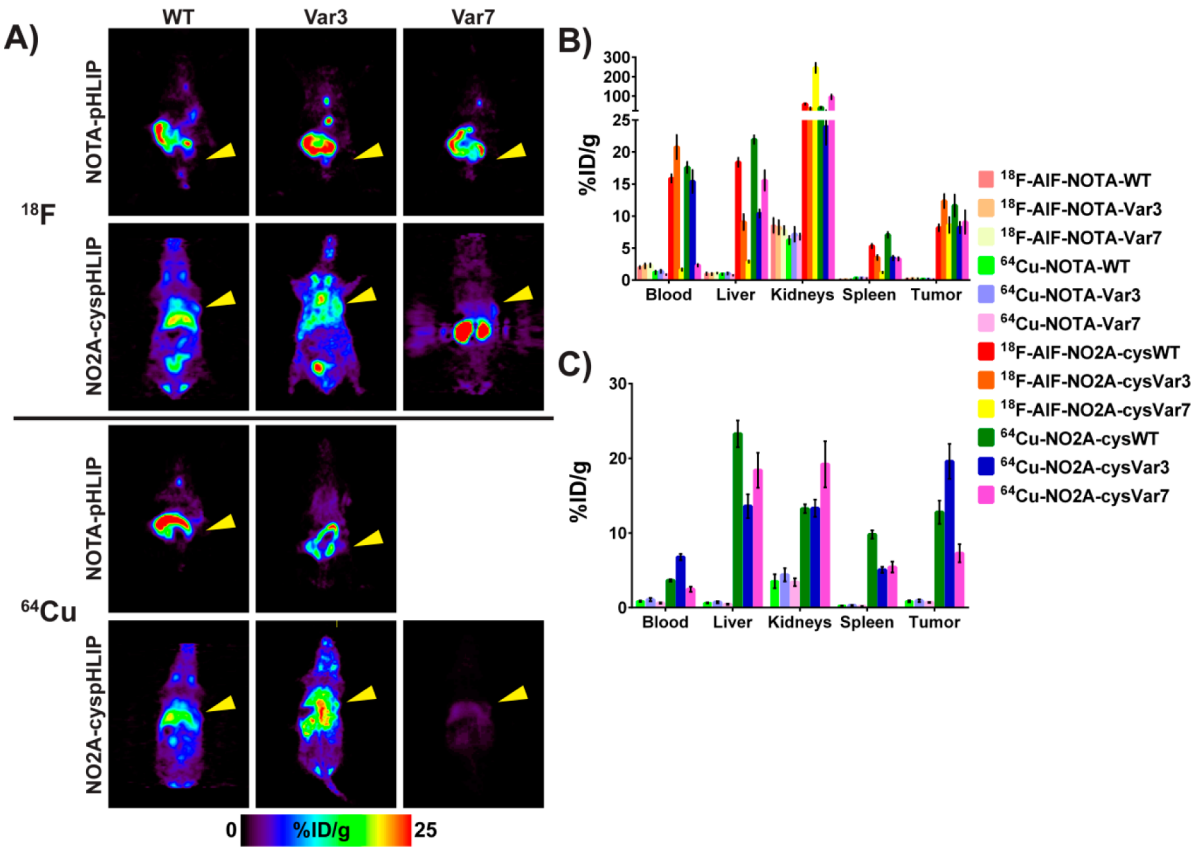

Figure 3. Coronal PET image slices at the level of the tumor at 4 h p.i. (A) and ex vivo biodistributions in selected organs at 4 h (B) and 24 h p.i. (C) showing differences in the tracer distribution in BALB/c female mice bearing 4T1 tumor allografts. The yellow arrowheads in (A) indicate where the tumor is located in the mouse. The selected scale on the PET images does not allow for tumor visualization in the case of the NO2A-cysVar7 constructs. Figure S2 shows the maximum intensity projections (MIPs) for these compounds at 4 h and the slices at the level of the tumor for the ^{18}F-AlF-NO2A-cyspHLIP constructs with a maximum value of 15%ID/g. Only ex vivo biodistribution data was obtained for ^{64}Cu-NOTA-Var7.

Table 1. Biodistribution (%ID/g) of the Six Radiolabeled N-Terminus Derivatized NOTA-pHLIP Derivatives in 4T1 Allografted Female BALB/c Mice at 4 h p.i.

tissue	^{64}Cu-NOTA-WT (n = 4)	^{64}Cu-NOTA-Var3 (n = 5)	^{64}Cu-NOTA-Var7 (n = 4)	^{18}F-AlF-NOTA-WT (n = 5)	^{18}F-AlF-NOTA-Var3 (n = 4)	^{18}F-AlF-NOTA-Var7 (n = 5)
blood	1.192 ± 0.263	1.371 ± 0.244	0.833 ± 0.068	1.978 ± 0.192	2.201 ± 0.374	2.292 ± 0.277
heart	0.50 ± 0.04	0.49 ± 0.05	0.35 ± 0.04	0.66 ± 0.12	0.78 ± 0.08	0.78 ± 0.06
lungs	1.414 ± 0.083	1.420 ± 0.117	0.996 ± 0.066	2.049 ± 0.211	2.217 ± 0.380	2.325 ± 0.212
liver	0.904 ± 0.097	1.034 ± 0.150	0.739 ± 0.041	0.973 ± 0.213	0.923 ± 0.153	1.089 ± 0.066
spleen	0.318 ± 0.023	0.340 ± 0.032	0.279 ± 0.016	0.434 ± 0.058	0.469 ± 0.093	0.485 ± 0.029
pancreas	0.261 ± 0.066	0.279 ± 0.041	0.198 ± 0.043	0.324 ± 0.059	0.332 ± 0.020	0.373 ± 0.051
stomach	0.282 ± 0.080	0.194 ± 0.050	0.300 ± 0.076	0.518 ± 0.152	0.482 ± 0.223	0.593 ± 0.153
s. intestine	0.391 ± 0.082	0.320 ± 0.042	0.307 ± 0.077	0.820 ± 0.245	0.927 ± 0.152	0.776 ± 0.196
l. intestine	9.96 ± 3.42	7.45 ± 2.73	7.78 ± 0.61	24.06 ± 2.85	22.05 ± 2.46	22.08 ± 6.02
kidneys	6.232 ± 0.613	7.165 ± 1.126	6.790 ± 0.461	8.550 ± 1.138	8.237 ± 1.106	7.759 ± 0.658
muscle	0.166 ± 0.008	0.171 ± 0.017	0.118 ± 0.025	0.283 ± 0.041	0.282 ± 0.055	0.325 ± 0.073
bone	0.274 ± 0.051	0.339 ± 0.018	0.229 ± 0.093	0.671 ± 0.305	0.540 ± 0.119	0.571 ± 0.202
skin	0.715 ± 0.109	0.775 ± 0.102	0.563 ± 0.145	1.032 ± 0.133	1.126 ± 0.115	1.377 ± 0.148
brain	0.054 ± 0.002	0.063 ± 0.011	0.042 ± 0.004	0.100 ± 0.015	0.107 ± 0.023	0.118 ± 0.011
tumor	0.679 ± 0.025	0.649 ± 0.091	0.546 ± 0.075	1.005 ± 0.232	0.923 ± 0.119	1.105 ± 0.125

the level of the tumor at 4 h p.i. of 11 of the 12 tracers tested and the ex vivo biodistribution in selected organs at 4 and 24 h p.i. (%ID/g, mean ± S.D.). The corresponding maximum intensity projections (MIPs) from the PET imaging study and the PET imaging slices at the level of the tumor with a lower maximum value for better visualization of the tumor at 4 h p.i. for the ^{18}F-AlF-NO2A-cyspHLIP constructs are collected in Figure S1. The 4 h ex vivo biodistribution values (%ID/g, mean ± S.D.) are collected in Tables 1 and 2 for all 12 radiopharmaceuticals, and the complete biodistribution results for all time points are tabulated in the Supporting Information (Tables S1−1 through S13−14). Due to the ex vivo biodistribution data for ^{64}Cu-NOTA-Var7 and the previous results from the imaging study of the other NOTA-pHLIP

DOI: 10.1021/acs.bioconjchem.6b00306
Bioconjugate Chem. 2016, 27, 2014−2023

Table 2. Biodistribution (%ID/g) of the Six Radiolabeled Cysteine Derivatized NO2A-cyspHLIP Derivatives in 4T1 Allografted Female BALB/c Mice at 4 h p.i.

tissue	^{64}Cu-NO2A-cysWT (n = 4)	^{64}Cu-NO2A-cysVar3 (n = 5)	^{64}Cu-NO2A-cysVar7 (n = 4)	^{18}F-AlF-NO2A-cysWT (n = 4)	^{18}F-AlF-NO2A-cysVar3 (n = 10)	^{18}F-AlF-NO2A-cysVar7 (n = 4)
blood	17.6 ± 0.86	15.4 ± 1.76	2.31 ± 0.18	15.9 ± 0.63	20.8 ± 1.88	1.64 ± 0.18
heart	5.52 ± 0.15	5.12 ± 0.63	2.68 ± 0.33	4.78 ± 0.53	6.29 ± 1.03	0.89 ± 0.12
lungs	12.3 ± 1.55	14.7 ± 0.93	4.21 ± 0.23	8.73 ± 0.84	11.8 ± 3.79	1.66 ± 0.07
liver	21.9 ± 0.64	10.4 ± 0.63	15.6 ± 1.58	12.6 ± 11.4	9.06 ± 1.24	2.90 ± 0.18
spleen	7.07 ± 0.44	3.45 ± 0.35	3.31 ± 0.24	5.31 ± 0.34	3.73 ± 0.66	1.19 ± 0.10
pancreas	3.00 ± 0.08	2.31 ± 0.25	1.84 ± 0.10	2.10 ± 0.43	2.44 ± 0.20	0.49 ± 0.03
stomach	1.82 ± 0.13	1.27 ± 0.35	3.33 ± 0.31	1.31 ± 0.96	1.29 ± 0.62	0.68 ± 0.10
s. intestine	4.56 ± 0.26	2.68 ± 0.24	6.37 ± 0.11	2.85 ± 0.31	2.06 ± 0.28	0.91 ± 0.03
l. intestine	4.09 ± 0.34	2.99 ± 0.20	8.19 ± 0.85	1.47 ± 0.14	2.07 ± 0.63	0.91 ± 0.12
kidneys	40.6 ± 4.04	24.0 ± 2.78	95.5 ± 11.9	59.1 ± 3.63	34.3 ± 6.91	246 ± 25.6
muscle	1.15 ± 0.08	1.10 ± 0.15	0.64 ± 0.07	1.23 ± 0.17	1.55 ± 0.27	0.35 ± 0.06
bone	3.04 ± 0.11	1.10 ± 0.14	1.57 ± 0.18	1.94 ± 0.45	1.66 ± 0.61	0.60 ± 0.12
skin	3.23 ± 0.12	3.43 ± 0.34	2.59 ± 0.05	2.85 ± 0.22	2.92 ± 0.71	1.59 ± 0.10
brain	0.62 ± 0.06	0.35 ± 0.07	0.25 ± 0.02	0.34 ± 0.06	0.52 ± 0.14	0.05 ± 0.01
tumor	11.7 ± 1.71	8.21 ± 0.86	9.07 ± 1.81	8.16 ± 0.53	10.6 ± 2.26	8.61 ± 1.21

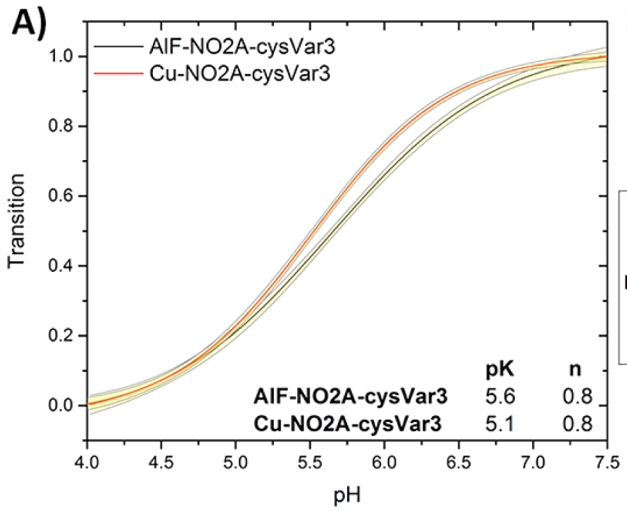

Figure 4. pH dependent bilayer insertion of NO2A-cysVar3 constructs. Changes in intrinsic construct fluorescence are used to measure the insertion of the construct population as a function of pH (transition from State II, at high pH, to State III, at low pH). Amount of construct population in State II is measured on the *y*-axis. 95% confidence intervals are indicated by yellow bands (A). pH-dependence parameters are used to calculate the percent of inserted construct population at various pH levels (B). These transitions were measured in the presence of physiological levels of free magnesium and calcium ions (0.65 mM and 1.25 mM, respectively).

constructs, an additional imaging study for ^{64}Cu-NOTA-Var7 was unjustified. These data clearly indicate that all constructs with the NO2A chelator far outperform the constructs with the NOTA chelator. It appears that NO2A-cyspHLIP constructs have a longer blood half-life, which results in higher targeting and longer retention within the tumor while the radiopharmaceutical clears from nontarget tissues and the blood.

Biophysical Studies. With 1-palmitoyl-2-oleoyl-*sn*-glycero-3-phosphocholine (POPC) liposomes as model membranes, our comparative biophysical investigation of the pH-dependent interaction of NOTA-pHLIP and NO2A-cyspHLIP constructs with the lipid bilayer indicated that NOTA constructs adopt unfavorable conformations at the membrane surface at physiological and low pH compared to NO2A constructs. Although biophysical measurements are typically conducted in solutions without the further addition of ions, we chose to investigate the performance of these constructs in both the absence and the presence of physiological levels of free magnesium and calcium ions. Wild-type constructs appear to be sensitive to the presence of divalent cations, most likely due to the multiple protonatable aspartic and glutamic acid residues at the inserting end of the peptide, which tend to form divalent complexes with these ions at physiological pH. Plots demonstrating the changes in fluorescence spectra of AlF-NOTA-Var3, Cu-NOTA-Var3, AlF-NO2A-cysVar3, and Cu-NO2A-cysVar3 upon interaction with membranes are shown in Figure S2.

Figure 3 shows the biodistribution of ^{64}Cu- and ^{18}F-NO2A constructs in selected tissues at 4 and 24 h. As previously reported,[17] Var7 constructs exhibit the fastest blood clearance with the highest signal in the kidneys at 4 h p.i. and kidney clearance at later time points. Both ^{18}F-AlF-NO2A-cysWT and ^{64}Cu-NO2A-cysWT have slightly higher liver and spleen uptake compared to the corresponding cysVar3 and cysVar7 conjugates. All of the NO2A constructs demonstrate a pH-dependent interaction with the lipid bilayer of the cellular membrane (Figures S3 and S4), but the NO2A-cysWT constructs exhibit the highest affinity to the lipid membrane

DOI: 10.1021/acs.bioconjchem.6b00306
Bioconjugate Chem. 2016, 27, 2014−2023

at physiological pH. Additionally, the p*K* of transition from the membrane-bound state to the inserted state is higher for NO2A-cysWT constructs compared with NO2A-cysVar3 and NO2A-cysVar7 constructs. This shift in p*K* is most likely responsible for the higher uptake of the NO2A-cysWT constructs by the liver and spleen.

Both ^{64}Cu-NO2A-cysVar3 and ^{18}F-AlF-NO2A-cysVar3 had the highest tumoral uptake, prolonged retention in the tumor, and minimal accumulation in other organs based on the ex vivo biodistribution data. Figure 4 shows the pH-dependent insertion and tabulates the percentage of the NO2A-cysVar3 construct population that is inserted in the membrane at various pHs. The results indicate that less than 5% of the lead compounds should be inserted into the membrane at pH 7.4 (physiological pH), whereas greater than 25% of the NO2A-cysVar3 compounds should be inserted into the cellular membrane at pH 6.0 (the approximate pH at the surface of cancer cells). In addition, the membrane insertion of Var3 and Var7 takes place at a rate 2 orders of magnitude higher than the rate of insertion of WT.[17]

In Vivo Studies in Prostate, Melanoma, and Brain Tumor Models. The two NO2A-cysVar3 compounds that showed superior targeting of the 4T1 tumors were compared in melanoma and prostate cancer models. Figure 5 shows the in vivo PET images of the uptake of the two tracers in tumors at 4 and 24 h p.i. The graph in Figure 6 directly compares the tumoral uptake of the two lead compounds at 4, 6, and 24 h p.i. for four of the tumor models investigated in this study. Due to the large variation in tumor size for the LNCaP tumors, the ex vivo data shows a minimal increase in tumoral uptake over the PC3 tumors, but both the murine B16−F10 melanoma tumors and 4T1 breast cancer tumors showed greater uptake of the tracers compared to the human prostate cancer models.

Because of the low uptake of the tracers in brain tissue, the ^{18}F-AlF-NO2A-cysVar3 was also evaluated in U87MG tumor-bearing mice. These tumors were implanted into the brain cavity or xenografted subcutaneously on the flank of nude mice. Figure S5 shows the imaging of these tumors. The uptake in the U87MG tumors that were implanted into the brain cavity showed significant uptake of the tracer in the portion of the tumor that was outside the skull. During necropsy, these tumors did not show significant infiltration of the brain. The ex vivo biodistribution of ^{18}F-AlF-NO2A-cysVar3 at 6 h p.i. in the nude mice with flank tumors is included in Figure S5. In order to conclusively determine if the uptake of ^{18}F-AlF-NO2A-cysVar3 was only in the portion of the tumor outside of the skull, a group of mice with GSC 5−22 tumors orthotopically xenografted behind an intact blood-brain barrier (BBB) were obtained. During necropsy, these tumors had infiltrated half of the brain, but there was no uptake observed in the PET image (Figure S5).

Specific Activity Investigation. The tracers were prepared to have comparable specific activities (approximately 100 μCi/nmol (3.7 MBq/nmol)) for most of the studies. A few additional studies were conducted with higher and lower specific activities in order to compare the effect of specific activity on tumoral uptake. The data sets were analyzed individually and showed that specific activity did not impact the biodistribution of the tracers, especially tumoral uptake. Thus, all of the data points for similar tumor models were averaged in aggregate (regardless of specific activity) and tabulated together in the Supporting Information.

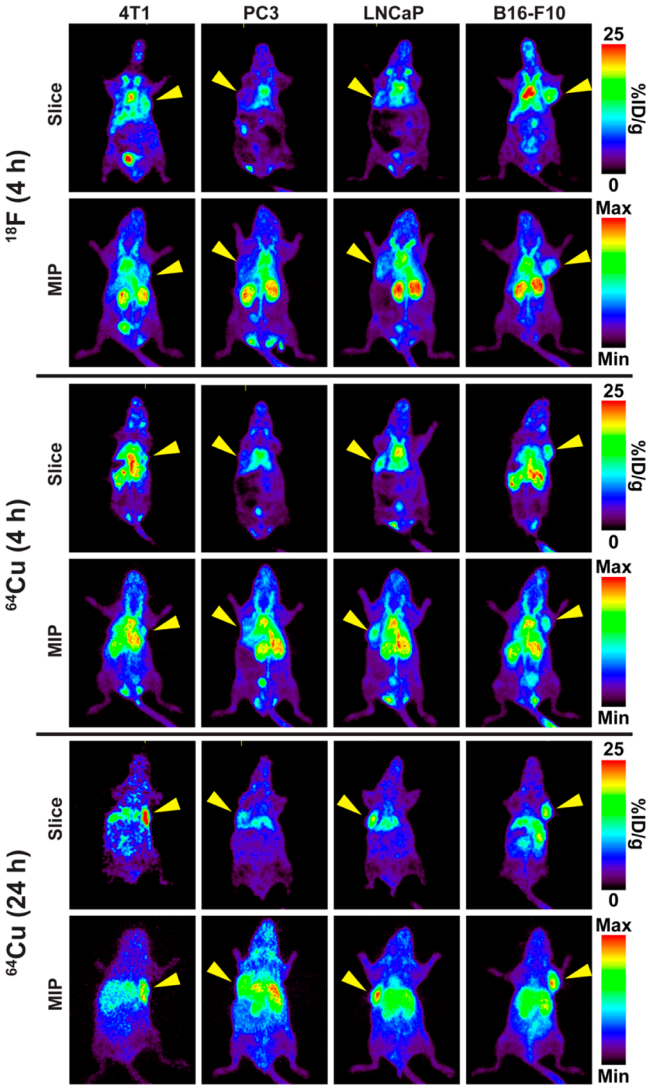

Figure 5. Slices and maximum intensity projections (MIP) from PET images showing differences in the radiolabeled NO2A-cysVar3 distribution at 4 and 24 h in BALB/c female mice bearing orthotopic 4T1 tumor allografts, nude male mice bearing shoulder PC3 or LNCaP xenografts, and C57Bl/6 female mice bearing orthotopic B16−F10 tumor allografts. The yellow arrowheads indicate where the tumor is located in the mouse.

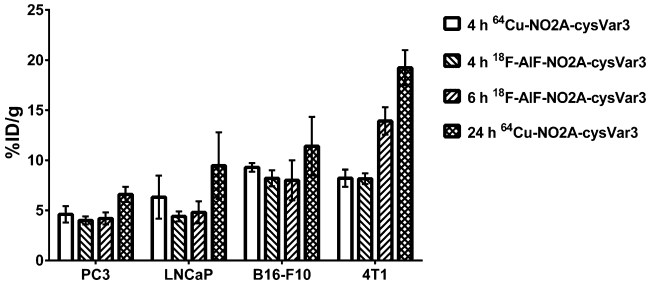

Figure 6. Graph of the ex vivo tumor uptake of the lead radiolabeled NO2A-cysVar3 in various tumor models at 4, 6, and 24 h p.i.

Tissue Autoradiography. The uptake of ^{64}Cu-NO2A-cysVar3 (24 h p.i.) in LNCaP and PC3 tumors was investigated via autoradiography with viable tissue stained with hematoxylin and eosin (H&E) to determine if the uptake was specific to regions showing indications of metabolic stress or necrosis.

DOI: 10.1021/acs.bioconjchem.6b00306
Bioconjugate Chem. 2016, 27, 2014−2023

Interestingly, uptake of ^{64}Cu-NO2A-cysVar3 appears to correlate with necrotic regions in LNCaP tumors, but not in PC3 tumors (Figure 7). This could be a result of the PC3

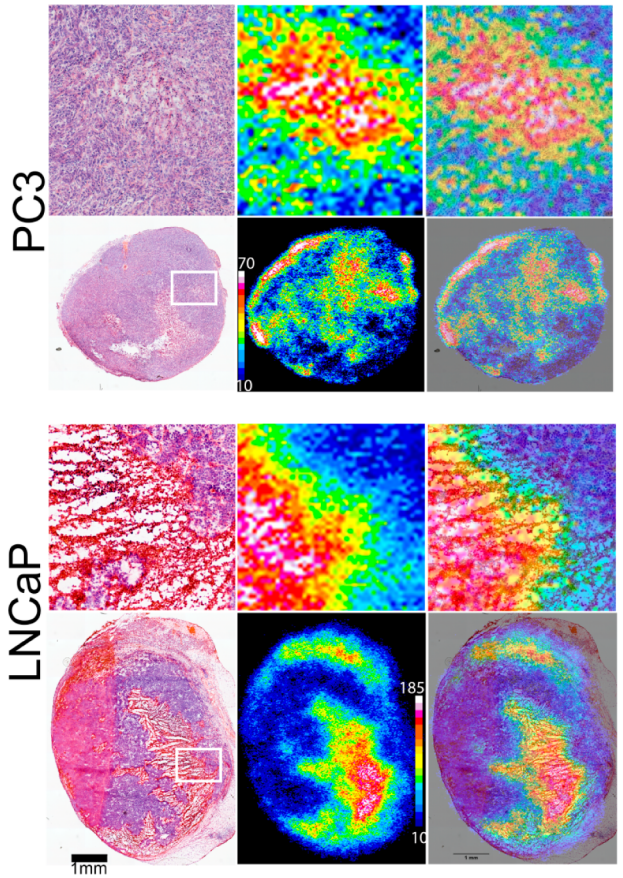

Figure 7. Comparison of uptake in sections of excised tumors from PC3 or LNCaP tumor-bearing male nude mice. The top panels are expansions of the whole tumor sections shown below. The left-most panels are H&E stained, the middle panels are the autoradiography, and the right-most panels are overlays.

tumors having less necrosis overall than the LNCaP tumors in this study. Additionally, the autoradiography shows increased relative uptake of ^{64}Cu-NO2A-cysVar3 (24 h p.i.) in LNCaP over PC3 tumors (Figure S6). This finding is similar to the results from previous studies by our group, in which both LNCaP and PC3 tumors were investigated.[10−12] H&E staining of tumor sections from 4T1 tumors excised 5−12 days post-inoculation show non-necrotic tumor tissue; thus, the greater tumoral uptake of the ^{64}Cu-NO2A-cysVar3 (according to the ex vivo biodistribution data) does not appear to be correlated to necrosis.

DISCUSSION

Two positron-emitting radionuclides (^{18}F and ^{64}Cu) can be used to label NOTA-peptides for in vivo imaging. While ^{64}Cu ($t_{1/2}$ = 12.7 h) has a moderately short half-life, the production of ^{64}Cu requires a higher energy cyclotron and expensive targetry with automated radionuclidic separation which many institutions do not currently have. Conversely, ^{18}F ($t_{1/2}$ = 109.8 min) is readily available from most medical cyclotrons and radiopharmaceutical centers, is routinely produced at numerous sites worldwide, and can be inexpensively concentrated for radiolabeling. Unlike conventional nucleophilic ^{18}F labeling of small organic molecules, using a chelator to coordinate the aluminum center of [^{18}F]-AlF is straightforward and can be done in aqueous solution.[15,16]

After the radiopharmaceuticals were successfully synthesized, their ability to target cancerous tissue was directly compared in 4T1 tumor-bearing female BALB/c mice. This model of triple-negative human stage IV breast cancer was chosen based on previous findings in our group that the pHLIP-PET agents were excreted through both the hepatobiliary and renal pathways and showed very good tumor:muscle ratios.[10−12] As such, breast cancer seemed an appropriate target which is imaged in humans away from these excretion organs. Additionally, previous results from Serganova et al. indicated that the pH of 4T1 tumors increases with increased size.[18] Thus, the 4T1 tumors in this study were purposely used 5−7 days after inoculation to ensure lower tumoral pH. The ex vivo biodistribution data show that the metalated NOTA-pHLIP variants are quickly cleared via both the hepatobiliary and renal pathways to reduce the overall circulating radioactivity significantly by 12 h p.i. The rapid excretion of the ^{64}Cu-NOTA-pHLIP variants from the intestines and slow elimination from the kidneys over time indicate that the compounds are not being taken up by the cells within these organs, but are being eliminated via these pathways. Additionally, when comparing the 2 h ex vivo data for kidneys-to-large intestine ratios [^{64}Cu-NOTA-WT is 0.35 ± 0.11; ^{18}F-AlF-NOTA-WT is 0.42 ± 0.03; ^{64}Cu-NOTA-var3 is 0.29 ± 0.12; ^{18}F-AlF-NOTA-var3 is 0.52 ± 0.15; ^{64}Cu-NOTA-var7 is 0.32 ± 0.07; ^{18}F-AlF-NOTA-var7 is 0.55 ± 0.19], there is no significant difference between the excretion pathways of variants radiolabeled with ^{64}Cu or ^{18}F. Perhaps the charge of the complexes appended to the pHLIP peptides helps to improve the elimination of these compounds, but also decreases the likelihood of uptake in low pH environments, such as the tumor, which may require more residence time in the blood. The lack of tumor targeting is evident in the imaging study results shown in Figure 3.

Conversely, the neutrally charged NO2A complexes conjugated to the cysteine residue of pHLIP peptides (which preserve their positive charge at the N-terminus) show prolonged blood circulation with slower clearance, consequently leading to better perfusion of the tracers in the tumor microenvironment where they are effectively trapped. The steady increase of the tumoral uptake of each of the tracers implies slow localization in the tumor site. The radiometalated NO2A-cysVar7 compounds had the shortest blood retention with similar tumoral uptake at 4 h to the other radiolabeled compounds. This rapid blood clearance may make the radiometalated NO2A-cysVar7 compounds useful for shorter imaging times (tumor is visible in the slices at the tumor level in Figure S1) as long as the tumor is sufficiently distant from the kidneys (the major organ visible in the MIP in Figure S1). The rapid clearance of the Var7 constructs (noted in previous studies[17,19]) may be a function of their physical characteristics. While these compounds have p*K*s of insertion similar to the NO2A-cysVar3 constructs, they are less hydrophobic than the NO2A-cysVar3 constructs. This lower hydrophobicity results in faster blood clearance (indicated by lower amounts of NO2A-cysVar7 constructs in the blood at every time point). The lower amount of radiolabeled compound in the blood for longer periods of time may result in lower tumoral uptake of the NO2A-cysVar7 constructs because the targeted tissue is exposed to less of the construct. At the same time, NO2A-

DOI: 10.1021/acs.bioconjchem.6b00306
Bioconjugate Chem. 2016, 27, 2014−2023

cysWT compounds exhibited highest accumulation in liver and spleen compared to NO2A-cysVar3 and NO2A-cysVar7, most probably due to their higher membrane affinity (greater hydrophobicity) at physiological pH and slower rate of membrane insertion.[17] Additionally, the ^{64}Cu-NO2A-cyspHLIP derivatives show decreased radioactivity accumulation in the kidney from 4 h p.i. to 24 h p.i. which is due to clearance of the drug rather than uptake, whereas the liver and spleen uptake remains similar for the two time points. The liver and spleen uptake may be due to loss of the ^{64}Cu from the chelator,[20] digestion of the radiotracer in vivo, or accumulation of intact tracer in these organs. Further investigation of this uptake is currently underway by investigating a pHLIPcys-NO2A derivative that contains the cysteine residue on the internalized portion of the peptide (C terminus), which could result in lower liver and spleen uptake if the uptake in these organs is due to loss of the ^{64}Cu from the chelator after membrane insertion.

From these results it becomes evident that introducing a benzene ring in close proximity to the N-terminus of the peptide sequence and using a negatively charged metal complex should be avoided in pHLIP peptide-mediated tumor imaging pharmaceuticals. Instead, conjugating to either the cysteine side chain or utilizing a suitable linking group on the N-terminus may improve tumor targeting of the synthesized pHLIP peptide. These general guidelines may help explain the improvements seen in this study and understand the results from previous studies.

Two compounds from the 12 tracers included in this study showed the greatest tumoral uptake and significant tumor-to-background contrast in the images throughout the imaging studies: ^{64}Cu-NO2A-cysVar3 and ^{18}F-AlF-NO2A-cysVar3. Therefore, we next investigated the in vivo properties of these two tracers in PC3 and LNCaP tumor-bearing mice to compare tumoral uptake with previous studies.[10−12] In these tumor models, the tumor accumulation of ^{64}Cu-NO2A-cysVar3 and ^{18}F-AlF-NO2A-cysVar3 was significantly higher compared to previous generations of PET isotope-labeled pHLIP constructs, especially at 24 h p.i. (Figure S7). Of particular note is the uptake of the ^{18}F-py-click-6Ahx-WT reported by Daumar et al.[11] and ^{68}Ga-DO3A-cysVar7 reported by Viola-Villegas et al.[12] Both of these previously reported compounds show significant uptake at 4 h p.i. and could be clinically useful. By comparison of the tumor:tissue ratios with those of previously reported compounds (Figure S8), the tumor:muscle ratios at 4 h p.i. were 7.4 ± 1.3 (^{64}Cu-NO2A-cysVar3), 6.9 ± 1.9 (^{18}F-AlF-NO2A-cysVar3), 4 ± 2 (^{18}F-py-click-6Ahx-WT), and 1.1 ± 1.5 (^{68}Ga-DO3A-cysVar7) in PC3 tumor-bearing male nude mice; the tumor:bone ratios were 2.7 ± 0.6 (^{64}Cu-NO2A-cysVar3), 3.2 ± 0.7 (^{18}F-AlF-NO2A-cysVar3), 1.3 ± 0.4 (^{18}F-py-click-6Ahx-WT), and 0.4 ± 0.3 (^{68}Ga-DO3A-cysVar7) in PC3 tumor-bearing male nude mice. Additionally, the tumor:muscle ratios in LNCaP tumor-bearing male nude mice at 4 h p.i. were 6 ± 2 (^{64}Cu-NO2A-cysVar3), 4.7 ± 0.9 (^{18}F-AlF-NO2A-cysVar3), and 6 ± 3 (^{18}F-py-click-6Ahx-WT); the tumor:bone ratios in LNCaP tumor-bearing male nude mice at 4 h p.i. were 4.2 ± 1.7 (^{64}Cu-NO2A-cysVar3), 4.3 ± 1.1 (^{18}F-AlF-NO2A-cysVar3), and 1.8 ± 0.6 (^{18}F-py-click-6Ahx-WT). In each of these cases, the tumor ratios of the two lead compounds from this study are much better than the ^{68}Ga-DO3A-cysVar7, which would result in improved image contrast. While the ^{18}F-py-click-6Ahx-WT had similar tumor:muscle ratios, the tumor:-bone ratios were much lower than the two lead compounds in both prostate cancer tumor models. The decreased tumor:bone ratios may indicate that the previously reported ^{18}F-py-click-6Ahx-WT was more prone to defluorination than the ^{18}F-labeled tracers presented in this study.

Despite the similar tumor-targeting properties, the preparation of ^{18}F-py-click-6Ahx-WT requires two HPLC-based separations and generates a volatile radioactive intermediate. The preparation of either of the lead compounds from this work, in contrast, did not required HPLC purification or heating beyond 80 °C which is optimal for rapid dose-on-demand production of the tracers for patient trials. Thus, the two lead compounds from this study appear to be the best candidates for clinical translation because of their improved biopharmaceutical properties and facile radiosynthesis.

Two other tumor types (melanoma and glioma) were included in this study to determine if the high uptake of these radiotracers seen in breast and prostate cancer models would translate to other types of tumors. The lead compounds have excellent tumor:background contrast in B16−F10 murine melanoma tumor-bearing mice, which was useful to identify very small tumors (<17 mg; ∼4 mm^3) in the PET image. Because of the contrast and high uptake, we plan to continue investigating the use of the two lead compounds in metastatic B16−F10 tumor models. For the brain tumor models, both an orthotopic and a subcutaneous (flank) brain tumor mouse model indicated that the ^{18}F-AlF-NO2A-cysVar3 was unable to penetrate an intact BBB, but was able to target brain tumors that had developed outside the BBB (Figure S5). Because this is a peptide-based tracer, we did not expect the compound to be able to cross an intact BBB; thus, these tracers may be useful in identifying metastases and possibly brain tumors in situations of compromised BBBs.

Previously, autoradiography was performed by Viola-Villegas et al. in prostate tumor sections from excised PC3 and LNCaP tumors in order to show differences in histology and tracer uptake;[12] thus, a similar study was performed with the uptake of ^{64}Cu-NO2A-cysVar3 in the same tumor lines. Overall, the ex vivo tumor sections show increased uptake of the ^{64}Cu-NO2A-cysVar3 in the necrotic regions of the LNCaP tumors (Figure 7). This may indicate that if necrosis is present, then uptake of ^{64}Cu-NO2A-cysVar3 may increase, but is not the only requirement. The findings here generally match the trend found by Viola-Villegas et al. in prostate tumor sections.[12] Additionally, the greater uptake in the allografted tumors may indicate the relative overall tumor environment is less acidic (higher) in the slower growing human cell lines investigated (PC3 and LNCaP), but is more acidic (lower) in the faster growing murine cell lines (B16−F10 and 4T1).

CONCLUSIONS

In our study, the NO2A-cysVar3 is the lead construct for clinical investigation. This construct can be radiolabeled with ^{18}F or ^{64}Cu with similar pharmacokinetic properties. The availability, limited dose exposure due to its short half-life, and cost effectiveness of ^{18}F supports the utility of ^{18}F-AlF-NO2A-cysVar3 in the clinic. Nevertheless, ^{64}Cu-NO2A-cysVar3 may be more suitable for inpatient imaging (where the patient will be in the clinic longer than 24 h) and in centers where the availability of the PET scanner may impact the time when patients are imaged. Clinical evaluation of these radiopharmaceuticals is currently underway.

DOI: 10.1021/acs.bioconjchem.6b00306
Bioconjugate Chem. 2016, 27, 2014−2023

EXPERIMENTAL SECTION

The D-amino acid versions of NOTA-derivatized pHLIP peptides were purchased from CS Bio (Menlo Park, CA) with ≥95% purity (combination of both chelators and three variants from Figure 2: NOTA-WT, NOTA-Var3, NOTA-Var7, NO2A-cysWT, NO2A-cysVar3, and NO2A-cysVar7). All other chemicals were purchased from commercial suppliers without further purification unless otherwise stated. Detailed method descriptions are found in the Supporting Information.

Radiochemistry. *General Labeling Methods for ^{64}Cu-NOTA-pHLIP.* Following a preparation similar to that of Zeglis et al.,[21] ^{64}Cu was diluted in a 100 mM NH_4OAc buffer (pH ∼ 5.5) and reacted with a NOTA-pHLIP derivative at 80 °C for 15 min.

General Labeling Methods for ^{18}F-AlF-NOTA-pHLIP. Following a modified labeling method described by Dijkgraaf et al.,[22] ^{18}F from the cyclotron target water was concentrated using a chromafix cartridge into 0.1 mL of 0.4 M $KHCO_3$ in metal-free water. The pH was adjusted and 0.1 mL AcN added. To this solution, $AlCl_3$ (80 nmol) in 0.1 M NH_4OAc buffer (pH ∼ 4.1) was added. After 5 min, the NOTA-pHLIP derivative was added and the reaction mixture reacted at 75 °C for 15 min.

General Purification. An Oasis HLB Plus Light or C18 Sep-Pak Light cartridge (Waters, Milford, MA) was used to remove unbound activity. The pure radiolabeled NOTA-pHLIP derivatives were eluted with EtOH and diluted with sterile phosphate buffered saline (PBS) with radiochemical purities >93% before administration to animals.

Animal Models. Animal studies were conducted according to an MSKCC IACUC-approved animal protocol. 4T1 (orthotopic breast cancer allografts of 1×10^6 cells surgically implanted in the mammary fat pad) and B16−F10 (orthotopic melanoma allografts of 1×10^5 cells injected intradermally on the shoulder) tumors were orthotopically inoculated in media in female BALB/c and C57Bl/6 mice (Charles River Laboratories (CRL)), respectively. Additionally, PC3 (3×10^6 cells) or LNCaP ($(3-6) \times 10^6$ cells) tumors were subcutaneously xenografted on the shoulder of athymic nude male mice (CRL). Mice were used once tumor volumes were approximately 90−300 mm^3.

In Vivo Animal PET Imaging and Biodistribution. Mice were injected with radiolabeled NOTA-pHLIP derivatives i.v. (500−700 μCi/mouse for PET imaging studies and 25−100 μCi/mouse for biodistribution studies). All injections were less than 200 μL with <10% EtOH in sterile PBS. PET images were obtained with the mice under anesthesia in an Inveon PET-CT or microPET Focus 120 (Siemens) at 0.5−48 h p.i. All images were analyzed using ASIPro VM (Concorde Microsystems). Dissections for ex vivo biodistribution were performed on mice after CO_2 asphyxiation or cervical dislocation while anesthetized at reported time points. Weight of the syringe prior to injection and after injection was used to determine the mass of injectate. Activity of the syringe prior to injection and after injection was used to determine the percent of injectate administered. The mass injected was corrected by the percent of radioactivity injected. Four to five aliquots (10 μL) were weighed and counted as internal standards for each study. All of the collected organs were counted using an automatic gamma counter (Wizard 3″, PerkinElmer, Waltham, MA). The total injected dose was found as the mass injected dose × fraction radioactivity injected × internal standard average counts/g. The percent injected dose (%ID) was determined as the counts for the tissue × 100/total injected dose. The %ID/g was calculated as the %ID/tissue weight. The average and standard deviation of the %ID and %ID/g was determined using normal methods ($n - 1$) for each set of mice.

Ex Vivo Autoradiography, Staining, and Microscopy. Tumors were excised from the mouse, embedded into Tissue-Plus O.C.T. (Scigen, Gardena, CA), stored at −20 °C until sectioning, and cut in sequential 10 μm sections. Select sections were exposed to autoradiography film (Fujifilm, GE Healthcare) for 1−3 days and read using a typhoon photographic film scanner (GE Healthcare). Additionally, sections were stained with H&E for gross tumor microscopy and then scanned.

Biophysical Studies. Biophysical studies were conducted on nonradioactive standards of the NOTA-pHLIP and NO2A-cyspHLIP compounds. All experiments were conducted with a 5 μM to 1 mM construct to lipid ratio. State I (construct with no liposomes in solution) and State II (construct in the presence of liposomes) were measured at pH 8; for State III (construct in the presence of liposomes), the pH of solution was dropped to pH 4 using 2 M HCl. Experiments were conducted in 10 mM phosphate buffer (Sigma-Aldrich) either without additional ions or in the presence of physiological levels of free magnesium and calcium (0.65 mM and 1.25 mM, respectively).

Liposome Preparation. Large unilamellar vesicles were prepared by extrusion. 1-Palmitoyl-2-oleoyl-*sn*-glycero-3-phosphocholine (POPC; Avanti Polar Lipids) was dissolved in chloroform at a concentration of 12.5 mg/mL, desolvated by rotary evaporation, and dried under high vacuum for 2 h. The phospholipid film was then rehydrated in 10 mM phosphate buffer (pH 8.0 with or without ions), vortexed, and extruded 15× through a 50 nm pore.

Steady-State Fluorescence. Tryptophan fluorescence spectra were measured using a PC1 ISS spectrofluorometer (Champaign, IL) with temperature control set to 25 °C. Fluorescence spectra were recorded with excitation and emission slits set to 1 mm, using an excitation wavelength of 295 nm, with excitation and emission polarizers set to 54.7° and 0°, respectively.

Steady-State Circular Dichroism. Circular dichroism measurements were taken using a MOS-450 spectrometer (Bio-Logic SAS, Claix, France) with temperature control set to 25 °C in the range of 190 to 260 nm with step of 1.0 nm.

pH Dependence. The pH-dependent insertion of the construct population was investigated using the shift in position of the wavelength of maximum intensity of the tryptophan fluorescence spectra varying pH conditions between 4 and 8. The pH after addition of HCl was measured using an Orion PerpHecT ROSS Combination pH Micro Electrode and an Orion Dual Star pH and ISE Benchtop Meter (Thermo Fisher Scientific). Tryptophan fluorescence spectra were recorded at each pH value and were analyzed using an online protein fluorescence and structural toolkit (PFAST) to obtain the positions of spectral maxima (λ_{max}). Finally, the positions of λ_{max} were plotted as a function of the various pHs and the Henderson−Hasselbalch equation employed to fit the data $\lambda_{max} = \lambda^2_{max} + \frac{\lambda^1_{max} - \lambda^2_{max}}{1 + 10^{n(pH-pK)}}$, where λ^1_{max} and λ^2_{max} are the positions of spectral maxima at the end and beginning of the State II − State III transition, respectively, n is the cooperativity parameter, and pK is the midpoint of transition.

DOI: 10.1021/acs.bioconjchem.6b00306
Bioconjugate Chem. 2016, 27, 2014−2023

■ ASSOCIATED CONTENT

Supporting Information

The Supporting Information is available free of charge on the ACS Publications website at DOI: 10.1021/acs.bioconjchem.6b00306.

Additional methods, figures, tables, and full biodistribution results from each radiotracer (PDF)

■ AUTHOR INFORMATION

Corresponding Author

*E-mail: lewisj2@mskcc.org. Tel: (646) 888-3038. Fax: (646) 888-3059.

Author Contributions

The manuscript was written through contributions of all authors. All authors have given approval to the final version of the manuscript.

Notes

The authors declare the following competing financial interest(s): Drs. Andreev, Engelman, Lewis and Reshetnyak have financial interests in pHLIP, Inc. Drs. Andreev and Reshetnyak have disclosed those interests fully to the University of Rhode Island. Dr. Engelman has disclosed those interests fully to Yale University. Dr. Lewis has disclosed those interests fully to the Memorial Sloan Kettering Cancer Center. Drs. Andreev, Engelman, Lewis and Reshetnyak have in place an approved plan for managing any potential conflicts.

■ ACKNOWLEDGMENTS

We appreciate the funding from NIH F32 CA186721 (D.W.D.), NIH R01 CA138468 (J.S.L.), the Academy of Finland (decision no. 278056, M.S.), NIH MSKCC Center Grant (P30-CA08748), and NIH Shared Instrumentation Grants (S10 RR020892−01 and S10 OD016207−01) for making this study possible. The authors would like to thank Prof. Fred K. Miller (Karmanos Cancer Institute, Detroit, MI) for his permission to obtain the 4T1 cancer cells and the Blasberg Lab (MSKCC, New York, NY) for providing us a frozen vial,[18] Alex Boleander (MSKCC, New York, NY) for providing U87MG tumor-bearing mice with tumors that were partially contained within the skull, and the Mellinghoff lab (MSKCC, New York, NY) for orthotopic GSC 5-22 tumors that were orthotopically implanted behind an intact BBB.

■ ABBREVIATIONS

AcN, acetonitrile; H&E, hematoxylin and eosin; MIP, maximum intensity projection; NOTA, 1,4,7-triazacyclononane-N′,N″,N‴-triacetic acid; pHLIP, pH (low) insertion peptide; pHLIP-PET, pHLIP radiolabeled with a positron emitting nuclide

■ REFERENCES

(1) Cairns, R., Papandreou, I., and Denko, N. (2006) Overcoming physiologic barriers to cancer treatment by molecularly targeting the tumor microenvironment. *Mol. Cancer Res. 4*, 61−70.

(2) Gatenby, R. A., and Gillies, R. J. (2004) Why do cancers have high aerobic glycolysis? *Nat. Rev. Cancer 4*, 891−899.

(3) Griffiths, J. R., McIntyre, D. J. O., Howe, F. A., and Stubbs, M. (2001) Why are cancer acidic? A carrier-mediated diffusion for H^+ transport in the interstitial fluid, In *The Tumor Microenvironment: Causes and Consequences of Hypoxia and Acidity* (Gillies, R. J., Ed.) pp 46−62, Vol. *240*, Novartis Foundation Symposia, John Wiley and Sons, Chichester.

(4) Andreev, O. A., Engelman, D. M., and Reshetnyak, Y. K. (2010) PH-sensitive membrane peptides (pHLIPs) as a novel class of delivery agents. *Mol. Membr. Biol. 27*, 341−352.

(5) Andreev, O. A., Engelman, D. M., and Reshetnyak, Y. K. (2014) Targeting diseased tissues by pHLIP insertion at low cell surface pH. *Front. Physiol. 5*, DOI: 10.3389/fphys.2014.00097.

(6) Andreev, O. A., Dupuy, A. D., Segala, M., Sandugu, S., Serra, D. A., Chichester, C. O., Engelman, D. M., and Reshetnyak, Y. K. (2007) Mechanism and uses of a membrane peptide that targets tumors and other acidic tissues in vivo. *Proc. Natl. Acad. Sci. U. S. A. 104*, 7893−7898.

(7) Viola-Villegas, N., Divilov, V., Andreev, O., Reshetnyak, Y., and Lewis, J. (2012) Towards the improvement of an acidosis-targeting peptide PET tracer. *J. Nucl. Med. 53*, 1673.

(8) Yao, L., Daniels, J., Wijesinghe, D., Andreev, O. A., and Reshetnyak, Y. K. (2013) PHLIP®-mediated delivery of PEGylated liposomes to cancer cells. *J. Controlled Release 167*, 228−237.

(9) Yao, L., Daniels, J., Moshnikova, A., Kuznetsov, S., Ahmed, A., Engelman, D. M., Reshetnyak, Y. K., and Andreev, O. A. (2013) pHLIP peptide targets nanogold particles to tumors. *Proc. Natl. Acad. Sci. U. S. A. 110*, 465−470.

(10) Vavere, A. L., Biddlecombe, G. B., Spees, W. M., Garbow, J. R., Wijesinghe, D., Andreev, O. A., Engelman, D. M., Reshetnyak, Y. K., and Lewis, J. S. (2009) A novel technology for the imaging of acidic prostate tumors by positron emission tomography. *Cancer Res. 69*, 4510−4516.

(11) Daumar, P., Wanger-Baumann, C. A., Pillarsetty, N., Fabrizio, L., Carlin, S. D., Andreev, O. A., Reshetnyak, Y. K., and Lewis, J. S. (2012) Efficient ^{18}F-labeling of large 37-amino-acid pHLIP peptide analogues and their biological evaluation. *Bioconjugate Chem. 23*, 1557−1566.

(12) Viola-Villegas, N. T., Carlin, S. D., Ackerstaff, E., Sevak, K. K., Divilov, V., Serganova, I., Kruchevsky, N., Anderson, M., Blasberg, R. G., Andreev, O. A., et al. (2014) Understanding the pharmacological properties of a metabolic PET tracer in prostate cancer. *Proc. Natl. Acad. Sci. U. S. A. 111*, 7254−7259.

(13) Carroll, V., Demoin, D. W., Hoffman, T. J., and Jurisson, S. S. (2012) Inorganic chemistry in nuclear imaging and radiotherapy: current and future directions. *Radiochim. Acta 100*, 653−667.

(14) Zeglis, B. M., Houghton, J. L., Evans, M. J., Viola-Villegas, N., and Lewis, J. S. (2014) Underscoring the Influence of Inorganic Chemistry on Nuclear Imaging with Radiometals. *Inorg. Chem. 53*, 1880−1899.

(15) McBride, W. J., D'souza, C. A., Sharkey, R. M., Karacay, H., Rossi, E. A., Chang, C.-H., and Goldenberg, D. M. (2010) Improved ^{18}F labeling of peptides with a fluoride-aluminum- chelate complex. *Bioconjugate Chem. 21*, 1331−1340.

(16) McBride, W. J., Sharkey, R. M., Karacay, H., D'Souza, C. A., Rossi, E. A., Laverman, P., Chang, C.-H., Boerman, O. C., and Goldenberg, D. M. (2009) A Novel Method of ^{18}F Radiolabeling for PET. *J. Nucl. Med. 50*, 991−998.

(17) Weerakkody, D., Moshnikova, A., Thakur, M. S., Moshnikova, V., Daniels, J., Engelman, D. M., Andreev, O. A., and Reshetnyak, Y. K. (2013) Family of pH (low) insertion peptides for tumor targeting. *Proc. Natl. Acad. Sci. U. S. A. 110*, 5834−5839.

(18) Serganova, I., Rizwan, A., Ni, X., Thakur, S. B., Vider, J., Russell, J., Blasberg, R., and Koutcher, J. A. (2011) Metabolic imaging: A link between lactate dehydrogenase A, lactate, and tumor phenotype. *Clin. Cancer Res. 17*, 6250−6261.

(19) Tapmeier, T. T., Moshnikova, A., Beech, J., Allen, D., Kinchesh, P., Smart, S., Harris, A., McIntyre, A., Engelman, D. M., Andreev, O. A., et al. (2015) The pH low insertion peptide pHLIP variant 3 as a novel marker of acidic malignant lesions. *Proc. Natl. Acad. Sci. U. S. A. 112*, 9710−9715.

(20) Bass, L. A., Wang, M., Welch, M. J., and Anderson, C. J. (2000) In Vivo Transchelation of Copper-64 from TETA-Octreotide to Superoxide Dismutase in Rat Liver. *Bioconjugate Chem. 11*, 527−532.

(21) Zeglis, B. M., Sevak, K. K., Reiner, T., Mohindra, P., Carlin, S. D., Zanzonico, P., Weissleder, R., and Lewis, J. S. (2013) A Pretargeted

DOI: 10.1021/acs.bioconjchem.6b00306
Bioconjugate Chem. 2016, 27, 2014−2023

PET Imaging Strategy Based on Bioorthogonal Diels-Alder Click Chemistry. *J. Nucl. Med. 54*, 1389−1396.
(22) Dijkgraaf, I., Franssen, G. M., McBride, W. J., D'Souza, C. A., Laverman, P., Smith, C. J., Goldenberg, D. M., Oyen, W. J. G., and Boerman, O. C. (2012) PET of Tumors Expressing Gastrin-Releasing Peptide Receptor with an ^{18}F-Labeled Bombesin Analog. *J. Nucl. Med. 53*, 947−952.

DOI: 10.1021/acs.bioconjchem.6b00306
Bioconjugate Chem. 2016, 27, 2014−2023